A High-Capacitance Salt-Free Dielectric for Self-Healable, Printable, and Flexible Organic Field Effect Transistors and Chemical Sensor

*Weiguo Huang, Kalpana Besar, Yong Zhang, Shyuan Yang, Gregory Wiedman, Yu Liu, Wenmin Guo, Jian Song, Kevin Hemker, Kalina Hristova, Ionnis J. Kymissis, and Howard E. Katz**

Printable and flexible electronics attract sustained attention for their low cost, easy scale up, and potential application in wearable and implantable sensors. However, they are susceptible to scratching, rupture, or other damage from bending or stretching due to their "soft" nature compared to their rigid counterparts (Si-based electronics), leading to loss of functionality. Self-healing capability is highly desirable for these "soft" electronic devices. Here, a versatile self-healing polymer blend dielectric is developed with no added salts and it is integrated into organic field transistors (OFETs) as a gate insulator material. This polymer blend exhibits an unusually high thin film capacitance (1400 nF cm^{-2} at 120 nm thickness and 20–100 Hz). Furthermore, it shows pronounced electrical and mechanical self-healing behavior, can serve as the gate dielectric for organic semiconductors, and can even induce healing of the conductivity of a layer coated above it together with the process of healing itself. Based on these attractive properties, we developed a self-healable, low-voltage operable, printed, and flexible OFET for the first time, showing promise for vapor sensing as well as conventional OFET applications.

Dr. W. Huang, K. Besar, G. Wiedman, Y. Liu, W. Guo, J. Song, Prof. K. Hemker, Prof. K. Hristova, Prof. H. E. Katz
Department of Materials Science and Engineering
The Johns Hopkins University
3400 North Charles Street, Baltimore, MD 21218, USA
E-mail: hekatz@jhu.edu

Dr. Y. Zhang, Prof. K. Hemker
Department of Mechanical Engineering
The Johns Hopkins University
3400 North Charles Street, Baltimore, MD 21218, USA

S. Yang, Prof. I. J. Kymissis
Department of Electrical Engineering
Columbia University SEAS
New York, NY 10027, USA

J. Song
State Key Laboratory on Integrated Optoelectronics
College of Electronic Science and Engineering
Jilin University
2699 Qianjin Street, Changchun 130012, P. R. China

Prof. H. E. Katz
Department of Chemistry
The Johns Hopkins University
3400 North Charles Street, Baltimore, MD 21218, USA

DOI: 10.1002/adfm.201404228

1. Introduction

Self-healable high-performance electronic materials have been intensively investigated in recent years. Early studies on self-healing materials were mainly focused on creation of self-repairable coatings and restoration of mechanical properties. For example, Abdullayev and co-workers developed self-healing coatings based on halloysite clay polymer composites for protection of copper alloys,[1] Sun's group successfully developed bioinspired self-healing superhydrophobic coatings by covalently attaching a fluoroalkylsilane layer,[2] Wudl and co-workers prepared a transparent organic polymeric material that can mechanically mend and "remend" itself under mild conditions;[3,4] Yoshie reported a bio-based furan polymer with self-healing ability from the reversible Diels–Alder reaction;[5] Chen's group prepared a self-healing system based on covalent dynamic gels;[6] and McCarthy and co-workers prepared a self-healing polymer (SHP) based on siloxane equilibration.[7] Later, researchers considered healable electronic properties simultaneously with mechanical properties. Bao and co-workers achieved the first repeatable, room-temperature self-healing electronic sensor skin;[8] later, they drastically increased the cycling lifetime of silicon microparticle anodes using self-healing chemistry.[9] White, Moore and co-workers restored film conductivity by embedding microcapsules filled with conductive agents.[10–14] Sun and co-workers successfully restored film conductivity just by applying a water drop to a damaged area.[15] Bielawski et al. developed a novel class of organometallic polymers comprising *N*-heterocyclic carbenes and transition metals that can be electrically healed.[16] There are many other examples of electrically healable materials.[17–20]

Recently, printable and flexible electronics have attracted sustained attention due to potentially low cost, easy scale-up, and potential application in wearable and implantable biochemical sensors.[21–31] Printable and flexible electronic components are more susceptible to scratching, rupture, or other damage from bending or stretching due to their "soft" nature compared to their rigid counterparts, such as Si-based electronics, resulting

in loss of functionality. Self-healing ability, an important feature of living creatures,[7–12] is highly desirable for these "soft" electronic devices. However, most research toward this goal has been limited to conductive media, such as conductive wire, film, and bulk materials;[8–15] there has been very little work on integrating self-healing materials into organic field effect transistors (OFETs), and especially not as gate insulators. Developing a material that simultaneously exhibits excellent dielectric properties for OFETs and autonomic mechanical self-healing behavior is still an unmet challenge. Although two reports introduce self-healing dielectric layers into organic field effect transistors, they only demonstrate the healing behavior following dielectric breakdown, rather than after both mechanical and electrical breakdown,[32,33] and the electrical self-healing process is relatively slow. Furthermore, these were not based on a potentially printable technology.

Here, we develop a versatile blend polymer system, poly(2-hydroxypropyl methacrylate)/poly(ethyleneimine) (PHPMA/PEI), as the first reported dielectric layer allowing self-healable, low-voltage-operable, printable, and flexible OFETs; this polymer blend shows surprisingly high capacitance (1400 nF cm^{-2} at 120 nm thickness and 20–100 Hz), much higher than all previously reported polymer dielectrics,[34–37] except for ion-gel dielectrics that contain more than 90% ions in the material.[38,39] Furthermore, this blend polymer system exhibits pronounced self-healing behavior, autonomically healing itself upon both mechanical and electrical breakdown. More importantly, it can even restore the conductivity of a gate electrode material coated above it simultaneously with the process of healing itself, without need for any added healing agent, which represents a significant step forward for development of fully healable electronics. Additionally, this dielectric layer shows promising application in improving the sensitivity of a gas sensor, such as for NH_3.

2. Results and Discussion

2.1. Material Design

In order to obtain a high performance self-healable material as dielectric layer for printable and flexible OFETs, the material should be readily soluble in common solvents, thus allowing solution processability. More importantly, high capacitance is desirable, as well as capability for repeated self-healing. Poly(methyl methacrylate) (PMMA) is a commonly used solution- processable dielectric; however, it has no self-healing ability under mild conditions due to lack of dynamic bonding and reversible reaction sites. Therefore, we chose its derivative, poly(2-hydroxypropyl methacrylate) (PHPMA), as an alternative (**Figure 1**); the introduction of the hydroxyl group will significantly strengthen interactions between polymer chains via numerous dynamic hydrogen bonds. However, this polymer shows a high glass transition temperature, above 100 °C, as shown by differential scanning calorimetry (DSC) (Figure S1, Supporting Information), indicating that the polymer chains have limited mobility at room temperature. In order to overcome this obstacle, we employ a more flexible polymer additive, poly (ethyleneimine) (PEI), which can interact with PHPMA through dynamic hydrogen bonds. The resulting blend polymer system shows an amorphous structure with a much lower glass transition temperature (below 40 °C). As a result, the polymer chains of the blend system have much higher freedom of motion at room temperature than PHPMA alone, which should significantly improve self-healing ability. Both poly (2-hydroxypropyl methacrylate) and poly (ethyleneimine) are readily soluble in ethanol, an environmentally friendly and inexpensive solvent, and an orthogonal solvent for

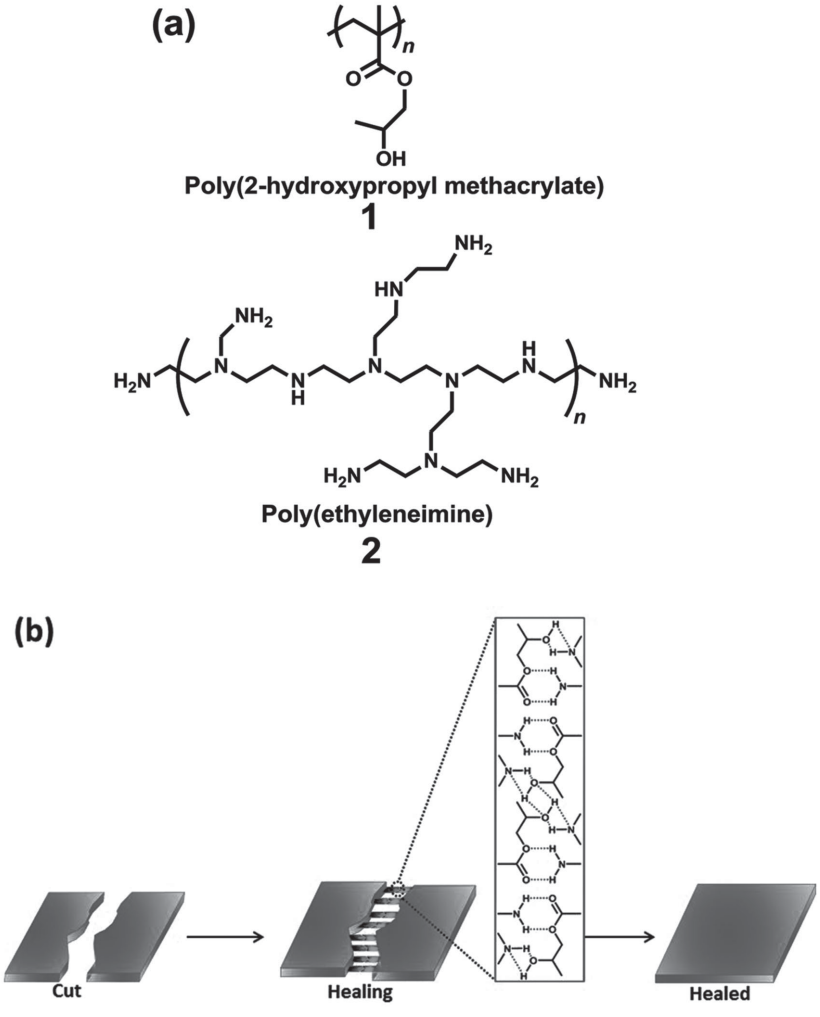

Figure 1. Chemical structure of polymers used for preparing self-healing polymer and illustration of polymer blend healing process. a) Chemical structure of **1**: poly(2-hydroxypropyl methacrylate) (PHPMA); **2**: poly(ethyleneimine) (PEI). b) Illustration of self-healing process of PHPMA/PEI blends polymer system, red and green connections represent robust hydrogen bonds between the severed surfaces.

most semiconductors,[40] meaning that our blend dielectric layer can also be easily coated on semiconductor films without causing damage. Also, most solvents for semiconductors, such as toluene, THF, chloroform, acetone, dichlorobenzene and dichloromethane, cannot dissolve the blend dielectric layer, providing us with a much more convenient and efficient way to manufacture devices with varied architectures.

2.2. Electrical Properties of the Blend Polymer System

2.2.1. Capacitance and Impedance

We used a metal–isolator–metal (MIM) architecture device (as shown in Figure S2, Supporting Information) for capacitance measurements; the results are shown in **Table 1** and **Figure 2**. While 20 Hz capacitance values are listed in the table, the figure shows that 80–90% of the capacitance is retained for thin films beyond 100 Hz. Polystyrene (PS) and poly(methyl methacrylate) (PMMA) show typical capacitance values as previous reports at a thickness around 100 nm,[38] PHPMA shows a higher capacitance value (66 nF cm^{-2}) than PS and PMMA at the same thickness range, and the value decreases proportionally with the increasing of film thickness, which is a typical feature for electron polarized dielectric materials. Surprisingly, after blending with PEI (2:1 weight ratio), the capacitance drastically increased up to 980 nF cm^{-2}; further increase of the PEI weigh ratio to 50% leads to a higher capacitance value of 1400 nF cm^{-2} (Figure S3, Supporting Information), which is higher than all the reported polymer dielectrics (except ion-gel dielectrics that contain more than 90% ions in the material).[34–39] The possible reason for the high capacitance is that the lone electron pair on nitrogen atoms in poly(ethyleneimine) may generate large dipoles when interacting with the OH groups on PHPMA.[41,42] Additionally, the capacitance value has less than the predicted dependence on film thickness; even a 16 µm thick film still exhibits a significantly high capacitance value of about 1000 nF cm^{-2} at 20–100 Hz. This is the first report of a neutral polymer maintaining such high effective capacitance at a macroscopic thickness, useful for robustness and printability. The capacitance decreases with increasing of frequency, as shown in Figure 2, similar to what is observed with ion-polarized dielectric materials.[38,39] From Figure 2, we noticed that the thickness dependence of capacitance per unit area is related to both PHPMA/PEI ratio and operating frequency. More specifically, at low frequency, <100 Hz, the capacitances of blend polymer film are largely independent of thickness, while films with very wide thickness range (from 120 nm to 16 µm) show a very narrow capacitance value distribution (650–1400 nF cm^{-2}). However, with increasing frequencies, the thickness dependence of film capacitance becomes more and more obvious. The possible reason for this phenomenon may be that, at low frequency, the proton transport contribution to the polarization can be completed through a macroscopic thickness, so a thicker film can show capacitance comparable to a thinner film. However, at higher frequency, transport-dependent polarization is incomplete, resulting in

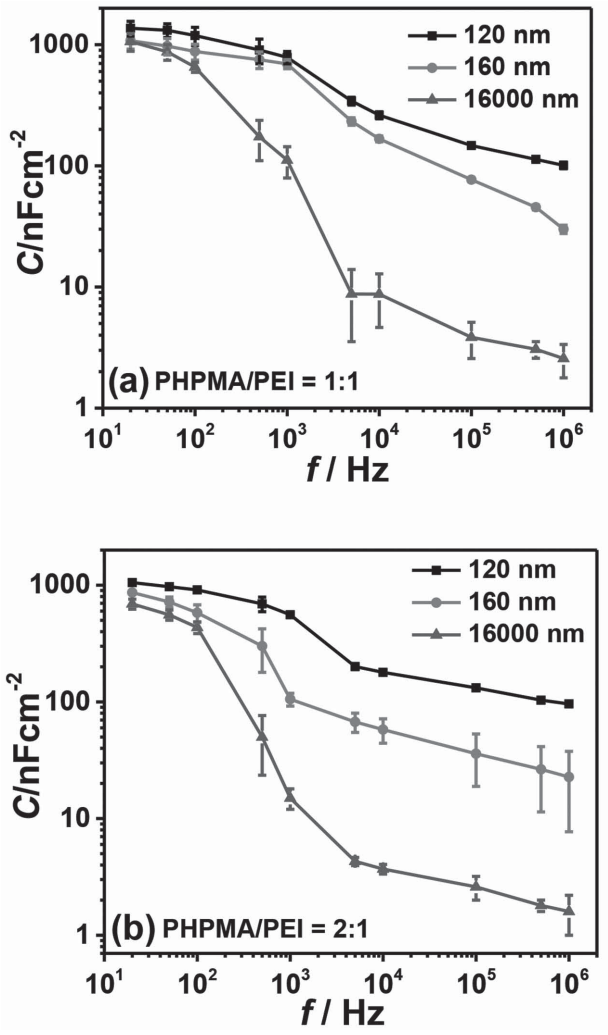

Figure 2. Capacitance frequency relationship at various thicknesses and different PEI ratios, a) PHPMA/PEI = 1:1; b) PHPMA/PEI = 2:1. The capacitance values were obtained from a MIM device configuration with an Agilent 4284A Precision LCR Meter. The frequency ranges from 20 Hz to 106 Hz.

Table 1. Capacitance value of different polymers with different thicknesses at 20 Hz. (All values are the average of at least ten samples).

Dielectric layer	Thickness [nm]	Capacitance [nF cm^{-2}] at 20 Hz
PS[a] [10 mg mL^{-1}]	100 ± 15	26 ± 2
PMMA[b] [10 mg mL^{-1}]	150 ± 20	20 ± 1
PHPMA[c] [10 mg mL^{-1}]	120 ± 20	66 ± 4
PHPMA [100 mg mL^{-1}]	1800 ± 200	5 ± 0.25
PHPMA + PEI[d] [10 mg mL^{-1}, 2:1][e]	120 ± 20	980 ± 160
PHPMA + PEI [100 mg mL^{-1}, 2:1]	3200 ± 200	900 ± 120
PHPMA + PEI [10 mg mL^{-1}, 1:1]	120 ± 20	1400 ± 250
PHPMA + PEI [20 mg mL^{-1}, 1:1]	160 ± 20	1050 ± 160
PHPMA + PEI [200 mg mL^{-1}, 1:1]	16 000 ± 1000	1060 ± 250

[a]PS: polystyrene; [b]PMMA: poly(methyl methacrylate); [c]PHPMA: poly(2-hydropropyl) methacrylate; [d]PEI: poly (ethyleneimine); [e]All are weight ratios.

a smaller capacitance value compared to thinner films. Furthermore, the PEI ratio also affects this thickness dependence behavior. In the blend polymer film with a higher PEI ratio, capacitance values show less thickness dependence, and in the blend polymer film with a higher PHPMA ratio, capacitance values show higher thickness dependence, as would be expected for typical dielectrics where capacitance is inversely proportional to film thickness.

We performed complex impedance measurements as shown in **Figure 3** in the frequency range from 0.1 Hz to 1 MHz. In Figure 3a, we use frequency as the horizontal axis and use two separate curves to display amplitude and phase of the frequency response. The $|Z|$ value increases on decreasing frequency, a typical capacitor behavior under AC test. At low frequency approaching the direct current (DC) condition, the capacitor shows very high resistivity, while at high frequency, the capacitor will become less resistive to AC voltage, and gradually becomes conductive as frequency keeps increasing. Figure 3b is a Nyquist plot that displays both amplitude and phase angle on a single plot, using frequency as a parameter in the plot. The semicircular plots of Z'' (image part) versus Z' (real part) indicate that the capacitor behavior approximates a parallel capacitor–resistor circuit (Rp and CPEp is Figure 3c).[43] Due to the starting point of this semicircular plot not being perfectly at Z' equal to 0, there should be a DC resistor with a small, but observable, resistance value.

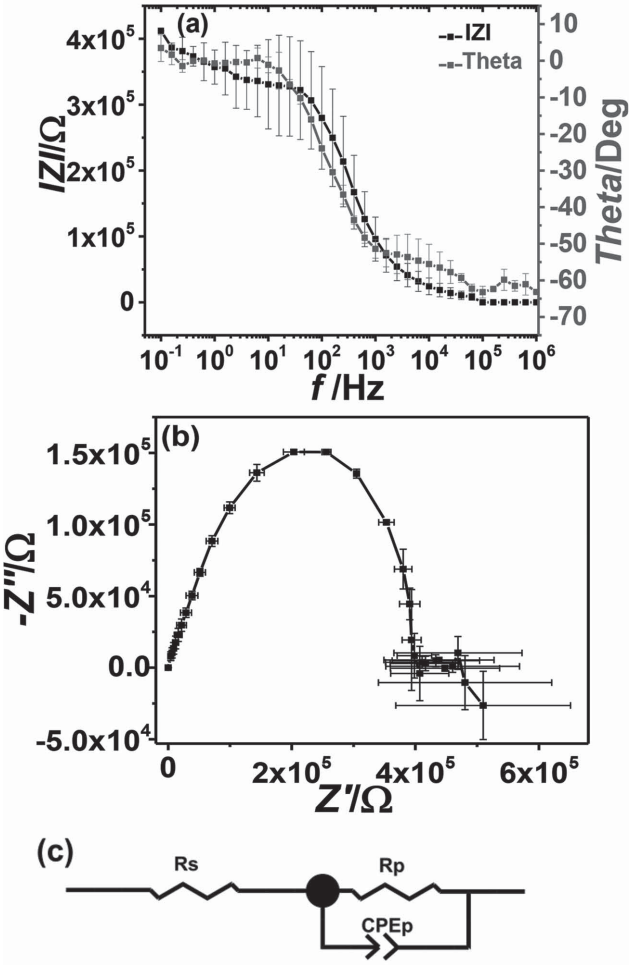

Figure 3. Impedance measurement. a) $|Z|$ value over frequency, b) Nyquist plot, and c) equivalent circuit of PHPMA/PEI (1:1) MIM capacitor.

2.2.2. Leakage Current Density Comparison

Figure S4 (Supporting Information) shows the leakage current densities of four different polymers under bias voltage (DC conditions) between ±5 V in MIM architecture devices. PHPMA/PEI blend polymer films show comparable leakage current with PMMA films at the same thickness range; furthermore, adding PEI to PHPMA decreases the leakage current density. These results support the hypothesis that PEI greatly eases the chain motion and leads to more uniform films with fewer pinholes through which leakage current could flow when the films are very thin. In the frequency-dependent capacitance measurements and the complex impedance measurements, both of which provide information about leakage current expressed as loss tangents, the loss seems to be at a minimum at 50–100 Hz, and rises considerably at 500 Hz and above. For further tests, we chose the PHPMA/PEI 1:1 blend since this ratio gives better performance, while higher PEI ratio (>50%) polymer blends were abandoned because of the formation of viscous gel-like films rather than a solid film, on which it is difficult to build devices.

2.2.3. Electrical Breakdown and Self-Healing Test

The capability of the gate dielectric to recover from electrical breakdown is vitally important to prevent permanent failure of an OFET. To test this capability in our material, we first measured the leakage current density between ±5 V bias voltages, then applied higher bias voltage (sweeping from 25 V to −25 V) to cause breakdown, after 1 min rechecked the leakage current densities under bias voltage between ±25 V to see whether these films are undergoing healing or further degradation, after 2 min, applied ±5 V bias voltages to measure the leakage current density level, and finally after 1 h, rechecked leakage current densities between ±5 V bias voltages and compared the results with the values before electrical breakdown to evaluate the electrical self-healing properties. As shown in Figure S5 (Supporting Information), before electrical breakdown, PHPMA/PEI shows comparable leakage current density (black curves) with the other three polymers. By sweeping bias voltage between ±25 V, electrical breakdown occurs in all four polymer films (leakage current density higher than 600 A cm^{-2}, red curves). After electrical breakdown for 1 min, sweeping bias voltage between ±25 V again, we observed PMMA, PS, and PHPMA films undergoing further degradation as evidenced by additional leakage current density increases (blue curves, clearer results were shown in the insert plots in Figure S5, Supporting Information), while only the PHPMA/PEI blend (1:1) film shows decrease in leakage current density, indicating that this blend polymer is healing itself immediately after electrical breakdown. After 2 min, we applied ±5 V bias voltages to measure the leakage

current density level, and only PHPMA/PEI blend (1:1) shows the leakage current density level decreasing toward its original value, while the other three polymers show no sign of recovering (pink curves). Finally, after 1 h, by applying bias voltage between ±5 V again, only the PHPMA/PEI blend (1:1) film shows leakage current level comparable with the value before electrical breakdown, while all three of the other polymer films show orders of magnitude higher leakage current densities than the value before breakdown (green curves). The PHPMA film completely lost its resistance, and no sign of healing could be observed. Another importance phenomenon is the leakage current density of PHPMA/PEI blend (1:1) decreasing over consecutively measurement cycles, as shown in Figure S5e (Supporting Information), indicating that the resistivity of the film is increasing over increasing test cycles. All these results clearly demonstrate that PEI could significantly improve resistance restoration in the PHPMA film, accomplishing electrical self-healing.

2.2.4. Performance of Self-Healing Polymer in Organic Field Effect Transistor as Dielectrics

In order to evaluate the performance of the self-healing polymer (PHPMA/PEI 1:1 blend) in OFETs when used as gate dielectrics, bottom-gated OFETs were fabricated on flexible ITO-coated PET substrates. Four conjugated molecules, pentacene, *N, N′*-bis(2-(pentafluorophenyl)ethyl)-1,4,5,8-naphthalene tetracarboxylic acid diimide (5FPE-NTCDI), poly(3-hexylthiophene) (P3HT), and quinacridone,[44] which cover the range of p- and n-type, small molecule and polymer, hydrophilic, and hydrophobic semiconductors, were employed to comprehensively assess the performance of PHPMA/PEI (1:1) blend self-healing polymer as a dielectric material. As a control, OFETs with PS, PMMA, PHPMA, and SiO_2 (no surface treatment) as dielectrics were also fabricated under exactly the same conditions as for the self-healing polymer, the only difference being that the OFETs with SiO_2 as dielectric were fabricated on rigid silica wafers, not on flexible PET substrates. Hydrophilic (highly polar) surfaces have generally been found to be unfavorable for charge carrier transport in OFETs due to their providing trap sites for electrons and holes,[40] decreasing mobility and increasing the threshold voltage. However, our self-healing polymer-based OFETs still show significantly higher drain current values with lower driving voltages than for OFETs using the other four dielectrics due to the much higher capacitance of the blend, as we can see from **Figure 4** (output curves of Figure 4 are shown in Figure S6 (Supporting Information); transfer curves for OFETs with the other four dielectrics are shown in Figures S7–S10, Supporting Information). Additionally, the mobilities of self-healing polymer (SHP)-OFETs and PHPMA-OFETs are usually higher than for OFETs using the other dielectric layers, as shown in Table S1 (Supporting Information). It is believed that larger charge carrier mobilities are observed from high charge density induced in the OFET channel.[38,40] Large carrier densities result in increased trap-filling and a general smoothing of electrostatic potential variations in the film due to trapped charge, and these combined effects may lead to higher carrier mobilities. Furthermore, SHP-based OFETs show excellent stability during storage under ambient conditions (pentacene for example, see Figure S11, Supporting Information) and negligible hysteresis behavior (Figure S12, Supporting Information), and still function well even after many cycles of bending. In order to quantitatively analyze the performance of SHP-OFETs under strain/stress, we use a home-built uniaxial stretcher (Figure S13, Supporting Information) to apply bending stress to flexible SHP-OFETs. In order to fully load strain/stress on the active device area, our device (P3HT/SHP-OFET) is located at the center of the flexible substrate where the strain/stress is maximized. The strain can be calculated by $\varepsilon = t/(2r + t)$,[45] where t is the thickness of the device and r is the bending radius. In our case, t is about 150 μm. At beginning, no bending stress is applied, ε value is 0%, the distance between the two ends of the flexible device is 2 cm; then, we reduced this distance to 1.5 cm, by measuring its bending radius (r = 3 mm), we calculated that the ε is about 2.5%. Then, we further push the stretcher to reduce the distance to 1.0 and 0.5 cm, with the corresponding bending radius of about 1.96 and 1.19 mm, respectively; we obtained 3.8% and 6.3% strain applied on the center of the device. The results are summarized in Table S2 (Supporting Information). At 2.5% and 3.8% strain, the drain current slightly increased, which is attributed to the increase of mobilities; the possible reason may be that the stress induced a certain degree of alignment of polymer chains in the P3HT film, thus increasing the mobilities. Only at 6.3% strain, the drain current and mobilities slightly decreased; this may be because of that much higher strain stress causes some separation of P3HT chains that would make the P3HT film less continuous, leading to decreased mobility. Also, the threshold voltage at higher strain (6.3%) decreased to −1.27 V, making the device lightly easier to turn on, one possible reason being that at this high strain value, the interface between the dielectric layer and the P3HT layer becomes smoother, which could eliminate some traps in the channel. After releasing the stress and returning to the original status, the performance of the flexible device shows slightly higher current and mobility, rather than degradation, indicating that the stress-induced P3HT film alignment could be retained after releasing the stress. After repeating this bending cycle 110 times, this P3HT/SHP-OFET still shows highly stable performance; the drain current mobility, threshold voltage, and on/off ratio are still comparable to the original values. All of the above results show that our flexible device can be stably operated under bending strain/stress.

We also demonstrate by using a manual model and actual inkjet deposition that the PHPMA/PEI blend polymer would be printable on flexible substrates and compatible with other printed OFET materials. The transfer and output curves of an all-manual-printed (using microliter syringes) and pneumatically printed dielectric OFETs with P3HT semiconductor are shown in Figure S14 (Supporting Information). The OFET shows excellent transistor behavior, with a high average hole mobility value of 0.16 $cm^2\ V^{-1}\ S^{-1}$, comparable to the value for a nonprinted P3HT/SHP-OFET. Comparable currents at similar voltages were achieved with pneumatic printing as well. The results indicated that this self-healing polymer dielectric is highly suitable for print-based fabrication. The details of all-printed, nonprinted, and pneumatically printed

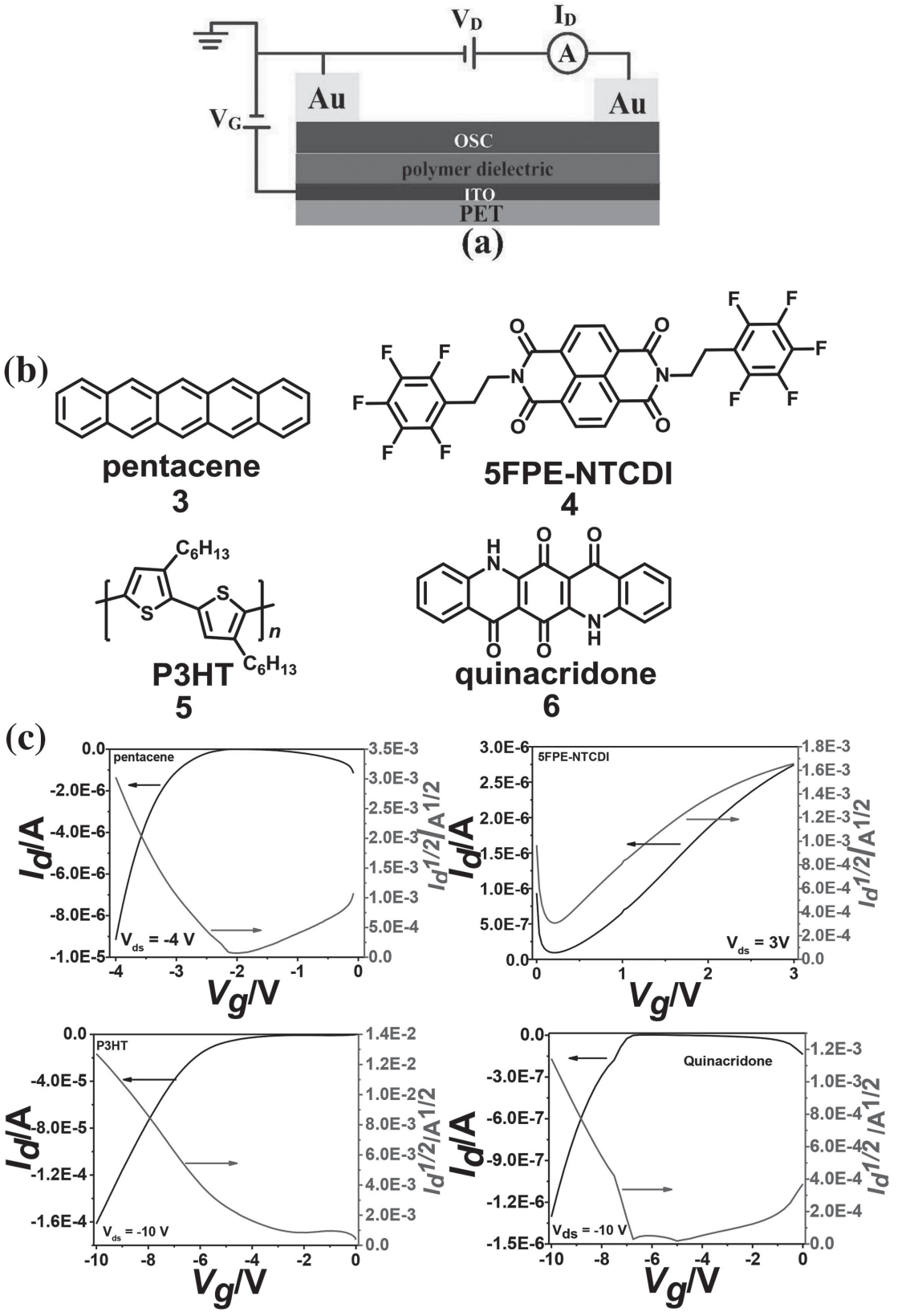

Figure 4. Performance of self-healing polymer in organic field effect transistor as dielectrics. a) Schematic diagram, b) chemical structure of four semiconductors, and c) *I–V* characteristics of SHP-OFETs. The devices have channel lengths of 250 μm and channel widths of 8000 μm. The gate voltage was swept at a rate of 50 mV s^{-1}.

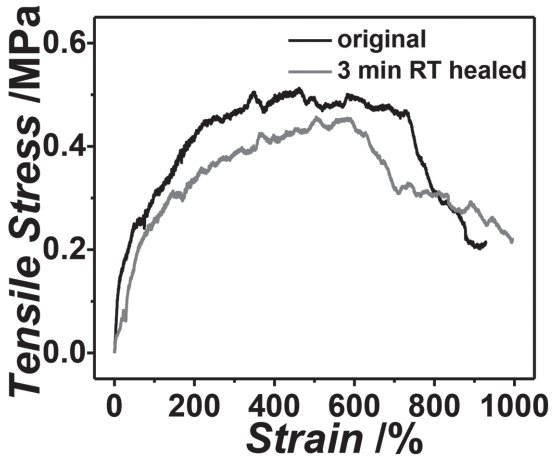

Figure 5. Test of mechanical self-healing of PHPMA/PEI 1:1. Tensile measurement of original polymer sample and severed sample after 3 min healing at room temperature; extension ratio 0.5 mm min^{-1}, load was measured with a resolution of 0.01 N and used to calculate the stress in the specimen. The specimens are about 1.5 cm in length, 0.3 cm in width, and 0.3 cm in thickness. The fluctuation of both curves may be caused by instant polymer chain relaxation in the specimens.

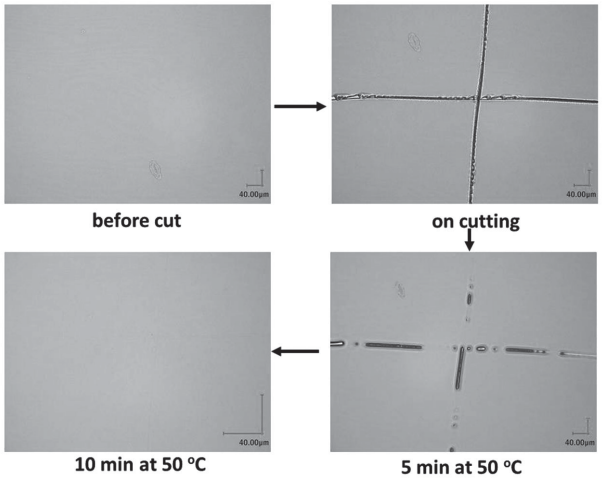

Figure 6. Optical monitoring of self-healing polymer PHPMA/PEI blend film healing process. The crossed black lines are cracks made with a blade; to clearly demonstrate that the crack is completely healed, the image of 10 min at 50 °C is further magnified compared with the other three images.

P3HT/SHP-OFET devices are summarized in Table S3 (Supporting Information).

2.3. Mechanical Properties of the Blend Polymer

Figure S15 (Supporting Information) shows the mechanical healing test of a coin-shape PHPMA/PEI (1:1) blend bulk sample; the dimensions are 1.5 cm in diameter and 0.3 cm in thickness. A blade was used to cut the sample into two pieces in the middle part, and then the severed surface was put back together with slight pressure. After 3 min in air under room temperature without adding any other healing agent, we applied tensile stress on it again, and the healed area still held together without any damage even at a large strain. **Figure 5** shows a more quantitative study of this self-healing polymer mechanical healing ability. As we can see, the self-healing polymer tensile stress can reach up to 0.5 MPa at a strain of 300%, well in the range of most reported self-healing polymers,[5–9] without immediate fracture after reaching its maximum tensile stress; instead, the tensile stress stays at 0.5 MPa until the strain reaches 750%. After that, the tensile stress starts to decrease slowly, finally showing fracture at 950% strain. A severed sample after 3 min healing in air at room temperature also shows comparable tensile stress level (close to 90% of original sample) at the same strain value, and the tensile stress can be continuous held until the strain reaches up to 600%, then starts decreasing slowly, and finally breaks at 1000% strain. This repeatable experiment clearly demonstrates that the self-healing polymer exhibits rapid self-healing behavior.

The PHPMA/PEI blend polymer film also shows excellent self-healing ability on scratching. In **Figure 6**, we made a PHPMA/PEI (1:1) film with a thickness about 10–11 μm, and then we made a cross scar on the film surface with a width of about 15 μm and a depth of 10 μm. After slightly warming the film at 50 °C for 5 min, the cross scar was partially healed, and after 10 min healing, the cross scar completely healed. The healing process could also be done at room temperature, but over slightly longer time. PS, PMMA, and PHPMA films cannot be completely healed even when heated at much higher temperatures (Figure S16, Supporting Information).

Based on this self-healing property of the PHPMA/PEI blend film, we further investigated its application on restoring conductivity of a conducting layer coated on it. Here, we coated a layer of carbon paint with a thickness of about 18 ± 5 μm directly on 18 ± 2 μm PHPMA/PEI blend polymer film, and then dried the bilayer under vacuum. Carbon paint was chosen because its solvent is isopropanol, which is similar to the solvent (ethanol) used for self-healing polymer deposition, so that during the drying process the two layers will partially diffuse into each other. We hypothesize that the resulting interlayer will be beneficial in healing the carbon paint layer and partially restore the conductivity.[46] As expected, as shown in **Figure 7**, before cutting, the carbon paint layer shows good conductivity; the surface resistivity is about 4.5 Ω cm; upon cutting, the resistivity drastically increased to over 9000 Ω cm; after 120 min healing at room temperature in air, the resistivity decreased to about 450 Ω cm; after 600 min, the resistivity is about 45 Ω cm, and the final resistivity is about 36 Ω cm, much closer to the original value than the value just after the cut (Figure S17, Supporting Information). This feature is highly promising since film conductivity restoration is much more difficult than for bulk conductors because we can easily contact severed surfaces of bulk materials, while reconnecting a severed film is much more challenging. Previous reports usually introduce healing agents (solvents) or embed microcapsules filled with conductive liquid into film to restore conductivity.[10,11] Our demonstration of conductivity restoration without any added agent is preferable for OFETs because we avoid delamination and degradation processes that could be associated with the additives.

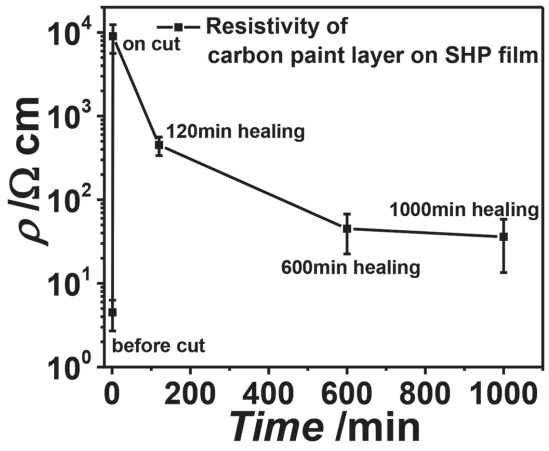

Figure 7. Carbon paint (coated on self-healing polymer) conductivity healing test. Data points represent means ± s.d. of at least five independent experiments.

2.4. Self-Healing Organic Field Effect Transistors

Based on this conductivity restoration ability conferred by the SHP, we further integrate both a self-healing polymer layer and a carbon paint layer into an OFET as a dielectric layer and a gate electrode, respectively, to manufacture a partially self-healing OFET. As shown in **Figure 8**, source and drain electrodes were patterned on a flexible PET substrate; then, the P3HT (10 mg mL^{-1} in dichlorobenzene) solution was drop cast on Au electrodes and annealed under low pressure N_2 at 90 °C for 3 h to form a semiconductor layer; 200 mg mL^{-1} PHPMA/PEI (1:1) ethanol solution was drop cast on P3HT film and dried under vacuum to form a 16 µm thick dielectric layer; finally, carbon paint suspension was coated on the self-healing dielectric layer as a gate electrode with a thickness of 18 ± 5 µm. The resulting top gate OFET shows excellent switching behavior at low operating gate voltage. Before cutting, drain current at −5 V is about −4.6 µA; upon cutting (no damage on P3HT), drain current decreases to −2.2 µA due to the damage to the lower conductance of the carbon paint layer. After healing at room temperature in air for 10 h, the carbon paint conductance was partially restored during the process of PHPMA/PEI dielectric healing itself, as discussed before, and we see the transistor drain current increased to −3.6 µA. The detailed information is summarized in Table S4 (Supporting Information). On cutting, the drain current and mobility decreased to 51% and 32%, the mobility decrease is probably due to the decrease of charge carrier density in the other half part of channel that is less connected with the gate probe. The threshold voltage also slightly shifted, and the on/off ratio decreased due to drain current changing to a smaller value. After healing, the drain current increased to 76% of its original value, the mobility also increased to 64% of its original value, threshold voltage changes toward its original value, and the on/off ratio also increased. This is the first report that multiple layers of an organic field effect transistor can automatically self-heal, a step toward fully self-healable electronic devices.

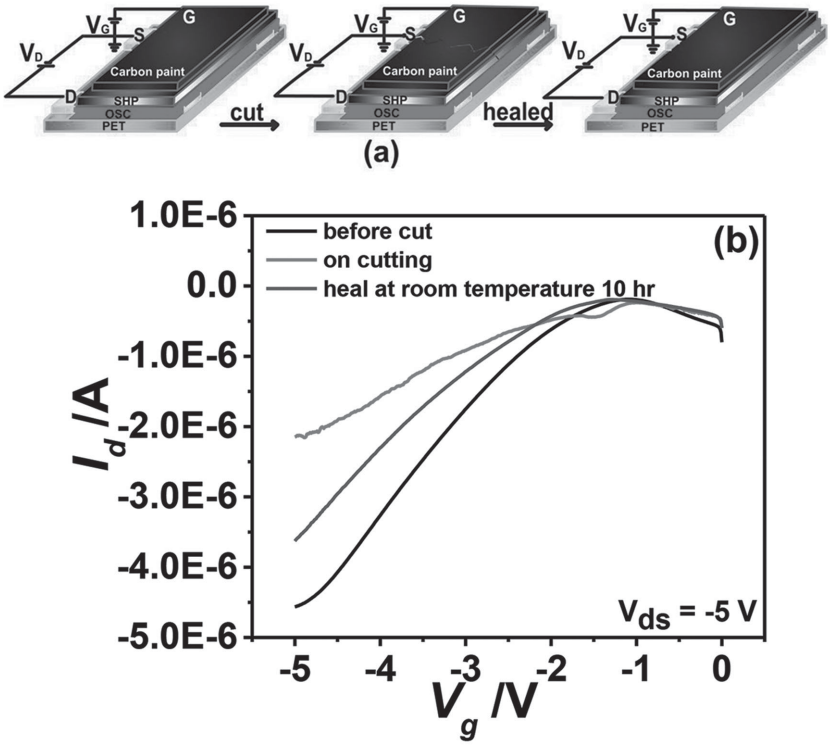

Figure 8. Self-healing organic field effect transistor. a) Schematic diagram of self-healing organic field effect transistor, the damage in gate electrode layer (carbon paint) can be partially healed together with the self-healing process of gate dielectric layer (SHP); and b) its transistor behavior (*I–V* characteristics) healing test.

2.5. Application in Flexible, Printable, and Low Voltage Operating OFET Sensors

Another significant application of this SHP-OFET is flexible, printable, and low-voltage operable OFET sensors. Here, we exposed a flexible P3HT OFET device with PHPMA/PEI (1:1) blend as a dielectric layer to 0.5 ppm NH_3, with operating voltage of −5 V. After 5 min exposure, the drain current decreased 23%, showing greater sensitivity than most reported P3HT NH_3 sensors.[47] The estimated limit of detection is much lower than 0.5 ppm. The possible reason for the higher sensitivity to NH_3 could be that this highly polar self-healing dielectric layer has significant affinity for NH_3, so the uptake of NH_3 by the sensor is increased, and more NH_3 can be adsorbed at the interface between the dielectric layer and the semiconductor layer (transistor channel), leading to a higher change of drain current. In order to verify this proposed mechanism, we used another semiconductor, 5FPE-NTCDI, instead of P3HT as a sensing layer. 5FPE-NTCDI is a highly stable semiconductor, and it shows negligible response to NH_3, except at higher concentrations (above 10 ppm);[48] as a control, 5FPE-NTCDI with PMMA as a dielectric layer was

also exposed to 0.5 ppm NH_3. After 5 min exposure, the 5FPE-NTCDI/PMMA device only gave 1% current increase, while the 5FPE-NTCDI/SHP device gives more than 5% current increase, a much higher response (Figure S18 and Table S5, Supporting Information). This result clearly demonstrated that this SHP-OFET is promising for highly sensitive, flexible, printable, and low-voltage operable OFET sensors.

3. Conclusion

In summary, we successfully developed a self-healing polymer blend based on PHPMA/PEI that shows electrical and mechanical self-healing ability; furthermore, this self-healing polymer exhibits surprisingly high effective thin film capacitance (up to 1400 nF cm^{-2} at thickness of 120 nm and 20–100 Hz) and the value shows negligible dependence on film thickness at this relatively low operating frequency. We then integrated the self-healing polymer into OFETs as a dielectric layer and achieved a self-healable, flexible, printable, and low-voltage operable OFET for the first time, which represents a major step forward to self-healable electronics. Finally, SHP-OFETs are highly promising for highly sensitive, wearable, implantable, and low-voltage operable OFET chemical sensors.

Our results illustrated that dielectrics with reversible intermolecular interactions (for example, dynamic H-bonding or reversible chemical reaction), and low glass transition temperature or some degree of molecule motion at room temperature are potentially applicable as self-healing gate materials for electronic devices. Furthermore, a high dielectric capacitance value is required to achieve low-voltage OFET operation; this is reachable in H-bonded materials from a small degree of proton transport. However, because hydrogen bonding groups also yield a highly polar surface that can trap charge carriers, a balance between the H-bond density and nonpolar groups (here, the methacrylate backbone) should be realized.

4. Experimental Section

Materials: P3HT (regioregular, average M_n 54 000–75 000, electronic grade, 99.995% trace metals basis) was purchased from Sigma-Aldrich; pentacene with 99.995% purity was purchased from Sigma-Aldrich and triple-sublimed before use; tetratetracontane (>98%) was purchased from Sigma-Aldrich; quinacridone with purity of 93% were purchased from TCI and sublimed five times before use; 5FPE-NTCDI was synthesized according to our previous publication.[49] Indium tin oxide-coated PET with surface resistivity 60 Ω sq^{-1}, poly(2-hydroxypropyl methacrylate), poly(ethyleneimine) (branched, $M_w \approx 25\,000$), poly(methyl methacrylate) ($M_w \approx 120\,000$), and polystyrene ($M_n \approx 192\,000$) were all purchased from Sigma-Aldrich. Conductive carbon paint was purchased from SPI Supplies. For spin-coating, P3HT (10 mg mL^{-1} in dichlorobenzene), PMMA (10 mg mL^{-1} in chloroform), PS (10 mg mL^{-1} in toluene), PHPMA (10 mg mL^{-1} in ethanol), PHPMA/PEI (10, 20, or 50 mg mL^{-1} each in ethanol in total) were prepared in a glove box filled with argon. More specifically, PHPMA and PEI were mixed in the desired ratio, most often 1:1, in ethanol at 10, 20, or 50 mg mL^{-1} concentrations of total solids. The mixtures were heated at 50 °C or lower (temperatures between 35 and 50 °C are permissible but temperatures above 50 °C should be avoided) with gentle stirring until a uniform mixture was obtained. The solutions were filtered through 0.2 μm filters before use.

Device Fabrication: Capacitors were prepared by spin coating polymers on ITO-coated glass at 1–2 krpm, with the highest capacitances obtained from 10 mg mL^{-1} total solid concentrations. Polymer films for electronic measurements (including capacitance, impedance, leakage current, breakdown, and gate dielectric characterizations) were annealed at 90–100 °C, taking care not to exceed 100 °C, for 60 min under N_2. Higher temperatures or extended heating in the presence of oxygen led to lower capacitance values, though 90 °C annealing of the thinnest films for 60 min under vacuum gave similar capacitances to those obtained from N_2 annealing. While the samples were not put into vacuum as a separate step, they were exposed to vacuum when semiconductors or electrodes were vapor-deposited. 50 nm thick Au top contacts were deposited through a shadow mask to form a 37 μm × 37 μm square electrode. OFETs were prepared on flexible substrates. Polymer dielectric was first spincoated on ITO-coated 127 μm thick PET thin sheets, then annealed at 90–100 °C for 1 h under N_2, and dried for 1 h under vacuum. Pentacene and 5FPE-NTCDI were thermally vapor deposited under high vacuum ≈3×10^{-6} Torr at a rate of 0.3 Å s^{-1} with final thickness of 50 nm. During the deposition, the substrates were held at 80 °C. The P3HT solution was spin-coated at a speed of 1000 rpm for 90 s, then annealed at 80 °C for 15 min in N_2, and dried for 1 h under vacuum. 50 nm Au source drain contacts were thermally vacuum deposited at ≈3×10^{-6} Torr. Quinacridone OFETs were fabricated according to the previous literature;[44] before quinacridone deposition, 30 nm $C_{44}H_{90}$ was first deposited on all five different dielectric layers because the low surface energy of the aliphatic $C_{44}H_{90}$ is critical for growth orientation of the H-bonded molecules, providing π-stacking parallel to the gate electrode and therefore high mobilities.[44] For the model all-printed device, first, we printed Ag nanoparticle ink (by dropcasting from a syringe in air, as was done for all the printing steps for this device) on a flexible thin PET sheet to form a 2 cm × 2 mm rectangular gate electrode, and dried at 50 °C for 30 min. PHPMA/PEI (200 mg mL^{-1}, 1:1) blend ethanol solution ink was printed on the Ag gate electrode to form an insulating film as a dielectric layer (≈16 μm thickness). The assembly was annealed under vacuum (≈0.05 atm) at 50 °C for 60 min). Subsequently, P3HT (10 mg mL^{-1} in dichlorobenzene) was printed on the dielectric layer. Finally, Ag nanoparticle ink was printed on the P3HT layer with channel length of 600 μm and channel width of 18 000 μm to form the source and drain electrodes. For the self-healing OFETs, we first thermally deposited 50 nm Au source drain contacts on flexible PET sheets at ≈3×10^{-6} Torr, then drop cast P3HT solution (10 mg mL^{-1} in dichlorobenzene) on Au electrodes, and annealed for 3 h at 90 °C in vacuum; then, the self-healing polymer (200 mg mL^{-1}, PHPMA/PEI blend) ethanol solution was drop cast on the P3HT layer to form a 16 ± 2 μm thick dielectric layer (annealed in vacuum (≈0.05 atm) at 50 °C for 60 min); finally 18 ± 5 μm carbon paint was coated on the self-healing polymer dielectric layer and dried under vacuum to form a gate electrode. Also, the mechanical self-healing test samples, because of their much greater thicknesses, were dried in vacuum (≈0.05 atm) at 50 °C for 24 h). The DSC sample was also dried under these conditions. All the device fabrication procedures are schematically shown in Figure S19 (Supporting Information).

Electrical and Mechanical Measurements: Electronic characterization of OFETs was conducted on an Agilent 4155C semiconductor parameter analyzer in open air. Capacitances were measured on an Agilent 4284A Precision LCR Meter; the impedance measurement was performed using a Solartron 1260 impedance analyzer from 0.1 to 10^6 Hz and Solartron 1287 electrochemical interface controlled by ZPlot and Zview software. Conductivity of carbon paint layers was measured by digital multimeter; thicknesses of films were determined by Dektak || A profilometer, and the film self-healing process was monitored by a REYENCE laser microscope. Tensile–stress tests were performed by using ASTM D638 normalized samples, with a strain rate of 0.5 mm min^{-1} at room temperature (25 °C), the dimensions of the samples are about 1.5 cm in length, 0.3 cm in width, and 0.3 cm in thickness. Load was measured with a resolution of 0.01 N and used to calculate the stress in the specimen. For self-healing experiments, the samples were cut by a blade, and the resulting severed samples were contacted again and

pressed by hand to make sure the severed surfaces were well in contact with each other. After 3 min healing at room temperature, the sample was subjected to the tensile–stress experiment. For conductivity healing experiments, the samples were cut by a blade to depth of about 26 ± 3 μm and a width of about 40 ± 5 μm. The resistivity was calculated by $R = \rho L/Wt$, where R is resistance, ρ is resistivity, L, W and t are the length, width, and thickness of measured area, respectively.

Sensing Experiments: 0.50 ppm NH_3 was obtained from diluting 5.00 ppm NH_3 with dry air; the dry air was purified by standard procedures before mixing with 5.00 ppm NH_3. The concentration was precisely controlled and displayed by an Environics SERIES 4040 gas dilution system. The total flow rate of gas is 1 L min^{-1}. The sensor devices were characterized before and after each exposure.

Supporting Information

Supporting Information is available from the Wiley Online Library or from the author.

Acknowledgements

The authors acknowledge primary funding from the Flextech Alliance. Additional support was provided by the Johns Hopkins Institute for Clinical and Translational Research. The dielectric property study was supported by the National Science Foundation, Division of Materials Research, Grant Number 1005398. We appreciate the availability of facilities of the Conte Nanotechnology Cleanroom lab at the University of Massachusetts-Amherst.

Received: November 28, 2014
Revised: March 19, 2015
Published online: May 12, 2015

[1] E. Abdullayev, V. Abbasov, A. Tursunbayeva, V. Portnov, H. Ibrahimov, G. Mukhtarova, Y. Lvov, *ACS Appl. Mater. Interfaces* **2013**, *5*, 4464.
[2] Y. Li, L. Li, J. Q. Sun, *Angew. Chem.* **2010**, *122*, 6265; *Angew. Chem. Int. Ed.* **2010**, *49*, 6129.
[3] X. Chen, M. A. Dam, K. Ono, A. Mal, H. Shen, S. R. Nutt, K. Sheran, F. Wudl, *Science* **2002**, *295*, 1698.
[4] S. D. Bergman, F. Wudl, *J. Mater. Chem.* **2008**, *18*, 41.
[5] C. Zeng, H. Seino, J. Ren, K. Hatanaka, N. Yoshie, *Macromolecules* **2013**, *46*, 1794.
[6] G. H. Deng, C. M. Tang, F. Y. Li, H. F. Jiang, Y. M. Chen, *Macromolecules* **2010**, *43*, 1191.
[7] P. W. Zheng, T. J. McCarthy, *J. Am. Chem. Soc.* **2012**, *134*, 2024.
[8] B. C.-K. Tee, C. Wang, R. Allen, Z. Bao, *Nat. Nanotech.* **2012**, *7*, 825.
[9] C. Wang, H. Wu, Z. Chen, M. T. McDowell, Y. Cui, Z. Bao, *Nat. Chem.* **2013**, *5*, 1042.
[10] S. R. White, N. R. Sottos, P. H. Geubelle, J. S. Moore, M. R. Kessler, S. R. Sriram, E. N. Brown, S. Viswanathan, *Nature* **2001**, *409*, 749.
[11] K. S. Toohey, N. R. Sottos, J. A. Lewis, J. S. Moore, S. R. White, *Nat. Mater.* **2007**, *6*, 581.
[12] S. A. Odom, M. M. Caruso, A. D. Finke, A. M. Prokup, J. A. Ritchey, J. H. Leonard, S. R. White, N. R. Sottos, J. S. Moore, *Adv. Funct. Mater.* **2010**, *20*, 1721.
[13] B. J. Blaiszik, S. L. B. Kramer, M. E. Grady, D. A. McIlroy, J. S. Moore, N. R. Sottos, S. R. White, *Adv. Mater.* **2012**, *24*, 398.
[14] S. A. Odom, S. Chayanupatkul, B. J. Blaiszik, O. Zhao, A. C. Jackson, P. V. Braun, N. R. Sottos, S. R. White, J. S. Moore, *Adv. Mater.* **2012**, *24*, 2578.
[15] Y. Li, S. S. Chen, M. C. Wu, J. Q. Sun, *Adv. Mater.* **2012**, *24*, 4578.
[16] K. Williams, A. Boydston, C. Bielawski, *J. R. Soc. Interface* **2007**, *4*, 359.
[17] M. Burnworth, L. Tang, J. R. Kumpfer, A. J. Duncan, F. L. Beyer, G. L. Fiore, S. J. Rowan, C. Weder, *Nature* **2011**, *472*, 334.
[18] P. Cordier, F. Tournilhac, C. Soulié-Ziakovic, L. Leibler, *Nature* **2008**, *451*, 977.
[19] R. Wool, *Soft Matter* **2008**, *4*, 400.
[20] Y. L. Chen, A. M. Kushner, G. A. Williams, Z. B. Guan, *Nat. Chem.* **2012**, *4*, 467.
[21] D.-H. Kim, N. Lu, M. Rui, Y.-S. Kim, R.-H. Kim, S. Wang, J. Wu, S. M. Won, H. Tao, A. Islam, K. J. Yu, T. Kim, R. Chowdhury, M. Ying, L. Xu, M. Li, H.-J. Chung, H. Keum, M. McCormick, P. Liu, Y.-W. Zhang, F. G. Omenetto, Y. Huang, T. Coleman, J. A. Rogers, *Science* **2011**, *333*, 838.
[22] S. C. B. Mannsfeld, B. C.-K. Tee, R. M. Stoltenberg, C. V. H.-H. Chen, S. Barman, B. V. O. Miur, A. N. Sokolov, C. Reese, Z. Bao, *Nat. Mater.* **2010**, *9*, 859.
[23] C. Pang, C. Lee, K.-Y. Suh, *J. Appl. Polym. Sci.* **2013**, *130*, 1429.
[24] M. Ramuz, B. C.-K. Tee, J. B.-H. Tok, Z. Bao, *Adv. Mater.* **2012**, *24*, 3223.
[25] T. Someya, T. Sekitani, S. Iba, Y. Kato, H. Kawaguchi, T. Sakurai, *Proc. Natl. Acad. Sci. U.S.A.* **2004**, *101*, 9966.
[26] M. Kaltenbrunner, T. Sekitani, J. Reeder, T. Yokota, K. Kuribara, T. Tokuhara, M. Drack, R. Schwodiauer, I. Graz, S. Bauer-Gogonea, S. Bauer, T. Someya, *Nature* **2013**, *499*, 458.
[27] T. Sekitani, U. Zschieschang, H. Klauk, T. Someya, *Nat. Mater.* **2010**, *9*, 1015.
[28] G. Schwartz, B. C.-K. Tee, J. Mei, A. L. Appleton, D. H. Kim, H. Wang, Z. Bao, *Nat. Commun.* **2012**, *4*, 2832.
[29] C. Wang, D. Hwang, Z. Yu, K. Takei, J. Park, T. Chen, B. Ma, A. Javey, *Nat. Mater.* **2013**, *12*, 899.
[30] S. Xu, Y. Zhang, L. Jia, K. E. Mathewson, K.-I. Jang, J. Kim, H. Fu, X. Huang, P. Chava, R. Wang, S. Bhole, L. Wang, Y. J. Na, Y. Guan, M. Flavin, Z. Han, Y. Huang, J. A. Rogers, *Science* **2014**, *344*, 70.
[31] R. C. Webb, A. P. Bonifas, A. Behnaz, Y. Zhang, K. J. Yu, H. Cheng, M. Shi, Z. Bian, Z. Liu, Y.-S. Kim, W.-H. Yeo, J. S. Park, J. Song, Y. Li, Y. Huang, A. M. Gorbach, J. A. Rogers, *Nat. Mater.* **2013**, *12*, 938.
[32] C. Dumas, R. E. Zein, H. Dallaporta, A. M. Charrier, *Langmuir* **2011**, *27*, 13643.
[33] C.-C. Lu, Y.-C. Lin, C.-H. Yeh, J.-C. Huang, P.-W. Chiu, *ACS Nano* **2012**, *5*, 4469.
[34] J. H. Li, Z. H. Sun, F. Yan, *Adv. Mater.* **2012**, *24*, 88.
[35] S. K. Hwang, I. Bae, S. M. Cho, R. H. Kim, H. J. Jung, C. Park, *Adv. Funct. Mater.* **2013**, *23*, 5484.
[36] K.-J. Baeg, D. Khim, S.-W. Jung, M. Kang, I.-K. You, D.-Y. Kim, A. Facchetti, Y.-Y. Noh, *Adv. Mater.* **2012**, *24*, 5433.
[37] C. Wang, W.-Y. Lee, R. Nakajima, J. Mei, D. H. Kim, Z. Bao, *Chem. Mater.* **2013**, *25*, 4806.
[38] a) J. H. Cho, J. Lee, Y. Xia, B. S. Kim, Y. He, M. J. Renn, T. P. Lodge, C. D. Frisbie, *Nat. Mater.* **2008**, *7*, 900; b) B. Pal, B. Dhar, K. See, H. E. Katz, *Nat. Mater.* **2009**, *8*, 898.
[39] a) K. H. Lee, M. S. Kang, S. Zhang, Y. Gu, T. P. Lodge, C. D. Frisbie, *Adv. Mater.* **2012**, *24*, 4457; b) G. Joshi, S. M. Pawde, *J. Appl. Polym. Sci.* **2006**, *102*, 1014.
[40] a) H. H. Fong, J.-K. Lee, Y.-F. Lim, A. A. Zakhidov, W. W. H. Wong, A. B. Holmes, C. K. Ober, G. G. Malliaras, *Adv. Mater.* **2011**, *23*, 735; b) R. P. Ortiz, A. Facchetti, T. J. Marks, *Chem. Rev.* **2010**, *110*, 205; c) P. G. Taylor, J.-K. Lee, A. A. Zakhidov, M. Chatzichristidi, H. H. Fong, J. A. DeFranco, G. G. Malliaras, C. K. Ober, *Adv. Mater.* **2009**, *21*, 2341; d) W. Huang, W. Shi, S. Han, J. Yu, *AIP Adv.* **2013**, *3*, 052122; e) W. Huang, K. Besar, R. LeCover, P. Dulloor, J. Sinha, J. F. M. Hardigree, C. Pick, J. Swavola, A. D. Everett, J. Frechette, M. Bevan, H. E. Katz, *Chem. Sci.* **2014**, *5*, 416.

[41] M. Salinas, C. M. Jäger, A. Y. Amin, P. O. Dral, T. Meyer-Friedrichsen, A. Hirsch, T. Clark, M. Halik, *J. Am. Chem. Soc.* **2012**, *134*, 12648.
[42] J. F. M. Hardigree, T. J. Dawidczyk, R. M. Ireland, G. L. Johns, B.-J. Jung, M. Nyman, R. Osterbacka, N. Marković, H. E. Katz, *ACS Appl. Mater. Interfaces* **2013**, *5*, 7025.
[43] a) Y. Liu, P. F. Guan, B. Zhang, M. L. Falk, H. E. Katz, *Chem. Mater.* **2013**, *25*, 3788; b) (Eds: A. Lasia, B. E. Conway, J. Bockris, R. E. White),, *Electrochemical Impedance Spectroscopy and Its Applications, Modern Aspects of Electrochemistry*, Kluwer Academic/Plenum Publishers, New York **1999**, Vol. *32*, p. 143.
[44] E. D. Glowacki, M. Irimia-Vladu, M. Kaltenbrunner, J. Gsiorowski, M. S. White, U. Monkowius, G. Romanazze, G. P. Suranna, P. Mastrorilli, T. Sekitani, S. Bauer, T. Someya, L. Torsi, N. S. Sariciftci, *Adv. Mater.* **2013**, *25*, 1563.
[45] C.-H. Yeh, Y.-W. Lain, Y.-C. Chiu, C.-H. Liao, D. R. Moyano, S. S. H. Hsu, P.-W. Chiu, *ACS Nano* **2014**, *8*, 7663.
[46] a) Y.-S. Kim, K.-S. Liao, C. J. Jan, D. E. Bergbreiter, J. C. Grunlan, *Chem. Mater.* **2006**, *18*, 2997; b) Y. Luo, Y. Li, Z. Li, *Smart Mater. Struct.* **2006**, *15*, 1979; c) X. weng, D. Brett, V. Yufit, P. Shearing, N. Brandon, M. Reece, H. Yan, C. Tighe, J. A. Darr, *Solid State Ionics* **2010**, *181*, 827; d) Z. Chen, J. C. M. Brokken-Zijp, H. P. Huinink, J. Loos, G. de With, M. A. J. Michels, *Macromolecules* **2006**, *39*, 6115; e) Y.-A. Li, Y.-J. Chen, N.-H. Tai, *Langmuir* **2013**, *29*, 8433.
[47] J. W. Jeong, Y. D. Lee, Y. M. Kim, Y. W. Park, J. H. Choi, T. H. Park, C. D. Soo, S. M. Won, I. K. Han, B. K. Ju, *Sens. Actuators B* **2010**, *146*, 40.
[48] W. Huang, J. Sinha, M.-L. Yeh, J. F. M. Hardigree, R. LeCover, K. Besar, A. M. Rule, P. N. Breysse, H. E. Katz, *Adv. Funct. Mater.* **2013**, *23*, 4094.
[49] H. E. Katz, A. J. Lovinger, J. Johnson, C. Kloc, T. Siegrist, W. Li, Y. Y. Lin, A. Dodabalapur, *Nature* **2000**, *404*, 478.